nature materials

SUPPLEMENTARY INFORMATION

DOI: 10.1038/NMAT4000

Anion charge storage through oxygen intercalation in $LaMnO_3$ perovskite pseudocapacitor electrodes

J. Tyler Mefford[1,§], William G. Hardin[2,§], Sheng Dai[3], Keith P. Johnston[2,4,5,*] & Keith J. Stevenson[1,2,5,*]

[1]Department of Chemistry, [2]Texas Materials Institute, [4]Department of Chemical Engineering, [5]Center for Electrochemistry, The University of Texas at Austin, 1 University Station, Austin, Texas 78712. [3]Chemical Sciences Division, Oak Ridge National Laboratory, Oak Ridge, TN 37831

* Correspondence should be addressed to: stevenson@cm.utexas.edu or kpj@che.utexas.edu

Experimental:

Peroxide studies of $LaNiO_3$: Electrodes were tested in a 0.1M KOH electrolyte that had been degassed with Ar for 15 min to purge the cell of oxygen. Then 150 µL of 10wt% H_2O_2 was added and immediately cyclic voltammetry was performed at a scan rate of 5 mV/s between the potentials 0.2 to -0.6V vs. Hg/HgO.

Oxygen reduction studies of $LaNiO_3$: Oxygen reduction activity of the electrodes was performed using rotating disk cyclic voltammetry in 150 mL of 0.1M KOH saturated with O_2 at a scan rate of 5 mV/s and a rotation rate of 1600 rpm.

Electrochemical Cycling of Carbon-Free $LaMnO_{3\pm\delta}$ Electrodes: In order to ensure sufficient sample sizes for XPS and XRD analysis, films of 1 mg/cm^2 were prepared by dispersing either $LaMnO_{3.09}$ or r-$LaMnO_{2.91}$ without any carbon additive in EtOH containing 0.05 wt% Na-substituted Nafion in a ratio of 2.5 mg mL^{-1} and sonicated for 30 min. 78.4 µL of this solution

DOI: 10.1038/NMAT4000

was spuncast at 700 rpm onto a glassy carbon electrode (0.196 cm^2, Pine Instruments). These electrodes were cycled in Ar saturated 1M KOH for 1, 25, 100, 250, and 500 cycles. After cycling, the electrodes were removed from the electrolyte and gently washed with DI water followed by drying under vacuum.

Surface Analysis of $LaMnO_{3\pm\delta}$: Due the semiconducting properties of $LaMnO_{3\pm\delta}$, charge neutralization must be employed during the collection of high resolution data. This minimizes, but does not eliminate, a global shift in the binding energies (BEs) for neat $LaMnO_{3\pm\delta}$ samples. To correct for these shifts, the Kratos AXIS Ultra DLD was first calibrated against the Ag 3d spectrum of freshly sputtered 99.99% pure Ag. Following spectrum calibration to Ag, the BE shifts due to $LaMnO_{3\pm\delta}$ charging were compensated by reconstruction of the La 3d 5/2 spectra, as outlined by Mickevicius *et al*.[1] This reconstruction procedure enabled us to shift the BE of the $LaMnO_{3\pm\delta}$ spectra relative to the deconvoluted La^{3+} 3d 5/2 peak with confidence, due to the electronic configuration of La^{3+} being that of xenon. Following these corrections, the O 1s spectra of both samples were deconvoluted utilizing Mickevicius *et al*. for H_2O and La-O peak assignments, De Asha *et al*. for La-OH assignment and Djurfors *et al*. for Mn-O and Mn-OH assignments.[1-4]

XPS of Electrochemically Cycled $LaMnO_{3.09}$ and r-$LaMnO_{2.91}$ Electrodes. *XPS of Electrochemically Cycled $LaMnO_{3.09}$ and r-$LaMnO_{2.91}$ Electrodes*. XPS data was acquired using a Kratos AXIS Ultra DLD spectrometer equipped with a monochromatic Al X-ray source (Al α, 1.4866 keV). Carbon-free electrodes of $LaMnO_{3.09}$and $LaMnO_{2.91}$ were electrochemically cycled, as previously described, for 25, 100 and 500 cycles. The active material on the electrode was removed,

washed with DI water and dried in a vacuum. To avoid signal convolution with the Nafion binder and provide a reference peak with which to calibrate the spectra, the Mn 2p 1/2 and La 4p 3/2 core regions where selected for analysis. The Mn 2p 1/2 region was used to avoid convolution with a copper LMM auger peak resulting from the copper tape on which each sample was mounted.[5] Where convolution did occur, the auger was fitted and removed prior to analysis. High resolution elemental analysis was performed on each sample, using a 20 eV pass energy, 0.1 eV step size and a 4 second dwell time. All spectra are the average of four collections. Charge compensation was used for the collection of all data, due to the lack of conductive carbon. To correct for shifts in binding energy due to charge compensation, peak reconstruction of the La 4p 3/2 region was performed as previously reported and the Mn 2p 1/2 region was shifted relative to the La 4p 3/2 $\underline{c}4f^0$ component.

XRD of Electrochemically Cycled $LaMnO_{3.09}$ and r-$LaMnO_{2.91}$ Electrodes: Structural information about cycled $LaMnO_{3\pm\delta}$ electrodes was obtained using wide-angle X-ray diffraction (Rigaku Spider, Cu Kα radiation, λ = 1.5418 Å) and analyzed with JADE software (Molecular Diffraction Inc.). Carbon-free electrodes were electrochemically cycled at 20 mV/s as described above for 1, 25, 100, 250, and 500 cycles. The active material on the electrode was gently rinsed free of residual electrolyte with DI water and dried under vacuum. The active material was then removed for XRD analysis.

DOI: 10.1038/NMAT4000

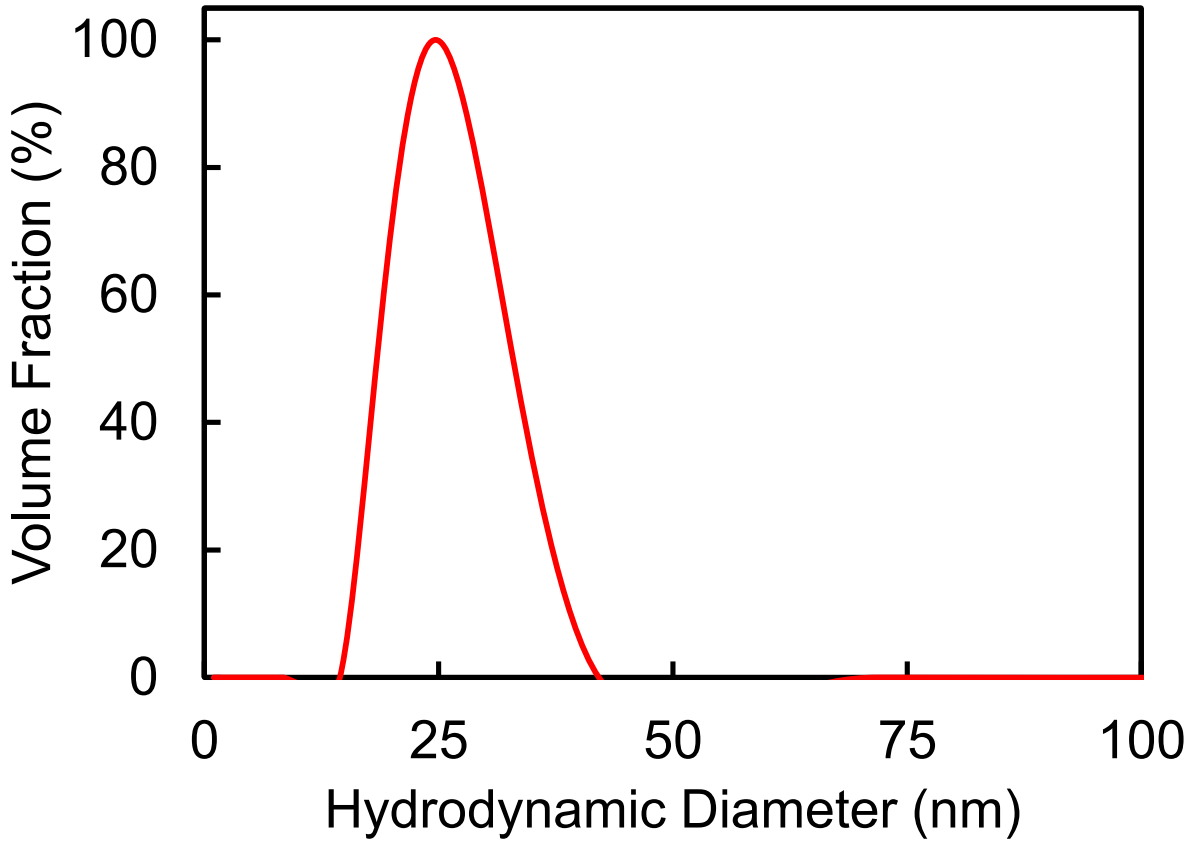

Figure S1 | Dynamic light scattering measurements of initial mixed metal hydroxides: During the reverse phase hydrolysis step of the synthesis, mixed metal hydroxides of La and Mn are formed. These mixed metal hydroxides may be individual particles or agglomerations with a hydrodynamic radius centered at 25 nm and a peak width of ± 7 nm. A small volume fraction of larger agglomerates is present as well with diameters between 75-100 nm.

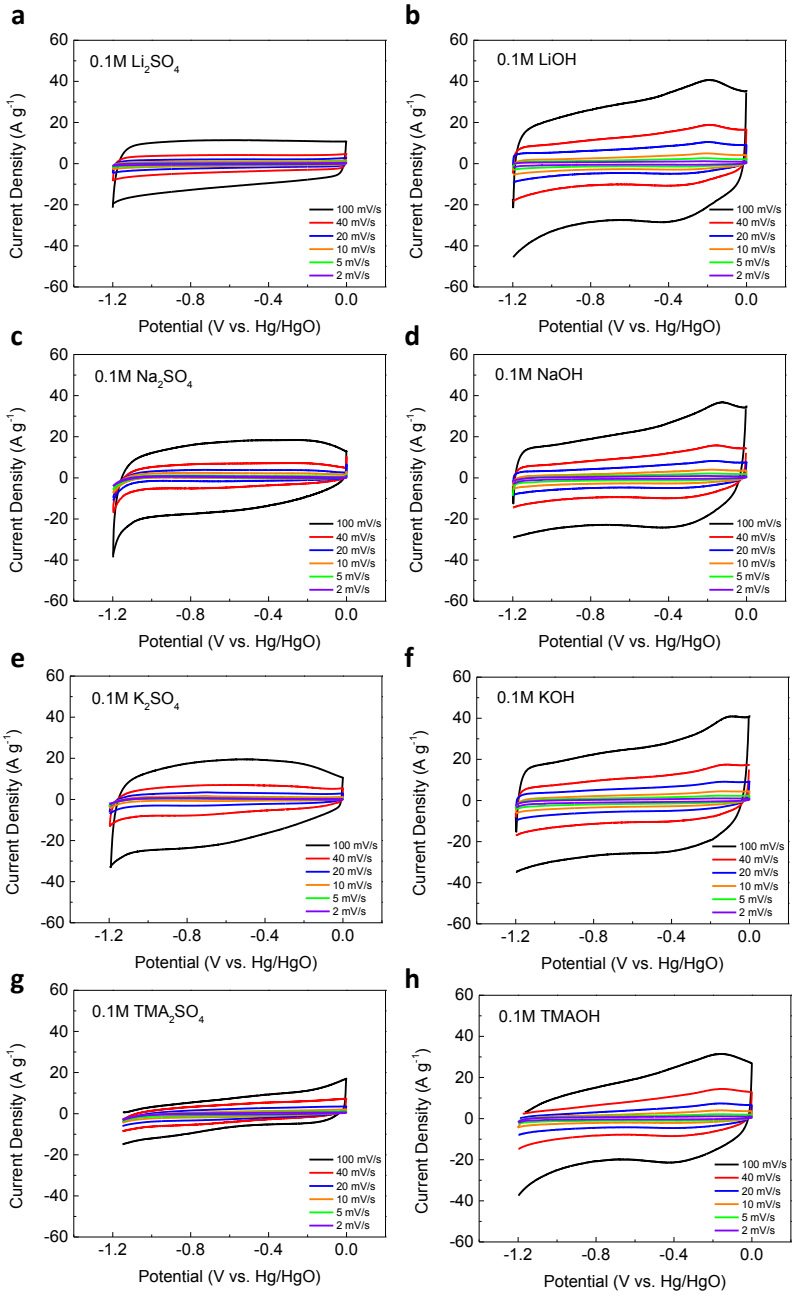

Figure S2 | Electrolyte studies of $LaMnO_{3+\delta}$: Cyclic voltammograms of $LaMnO_{3+\delta}$ in 0.1M sulfate based electrolytes in order of cationic radius Li^+ (**a**), Na^+ (**c**), K^+ (**e**), TMA^+ (**g**) compared to cyclic voltammograms of $LaMnO_{3+\delta}$ in 0.1M basic electrolytes in order of cationic radius Li^+ (**b**), Na^+

DOI: 10.1038/NMAT4000

(**d**), K^+ (**f**), TMA^+ (**h**). In all of these CV's, the current contribution from the N-OMC carbon support has been subtracted. The presence of both oxidation and reduction peaks in the 0.1M basic electrolytes is demonstrative of the role of OH^- ions as intercalating species in $LaMnO_{3.09}$.

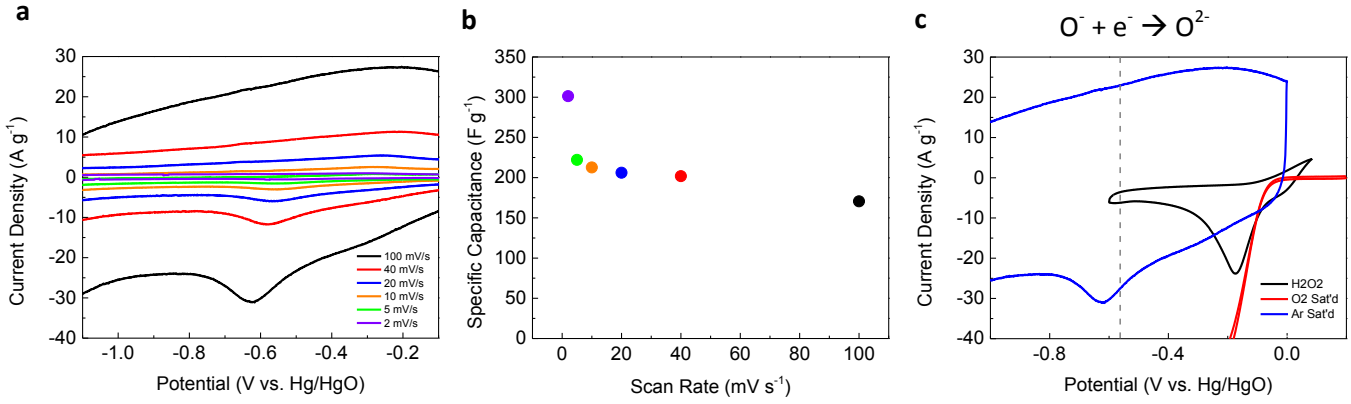

Figure S3 | Capacitive responses of $LaNiO_3$. a,b. (**a**) Cyclic voltammogram and (**b**) specific capacitance versus scan rate for $LaNiO_{3-\delta}$. **c,** Overlay of hydrogen peroxide voltammogram at 5 mV/s, oxygen reduction at 5 mV/s and a rotation rate of 1600 rpm, and the pseudocapacitive CV curves at 100 mV/s for $LaNiO_3$ The large peak in the peroxide curve corresponds to reduction of O_2 from the chemical disproportionation of H_2O_2. The upturn at ~-0.6V corresponds to the reduction of the peroxide species (also indicated by the dashed line).

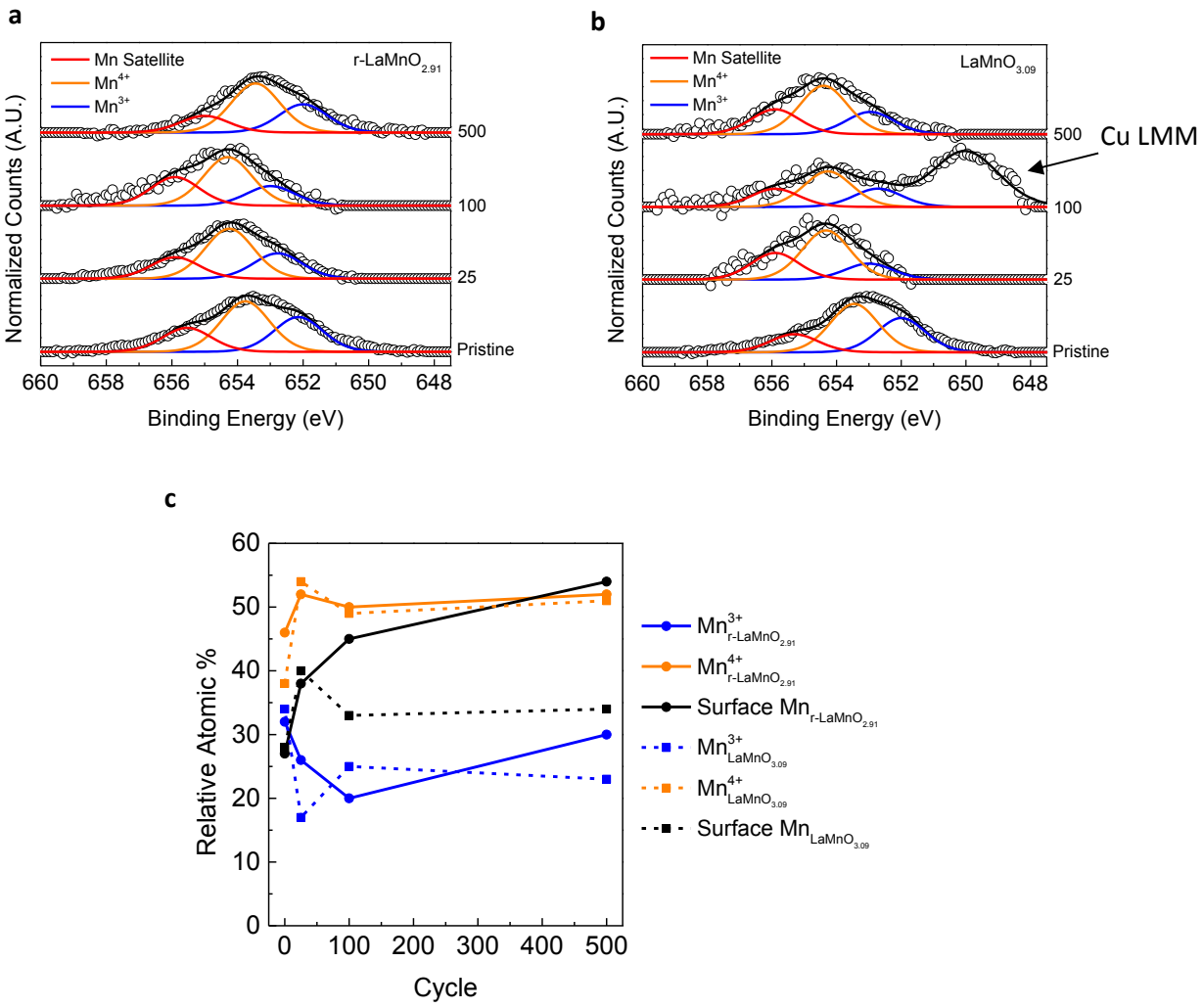

Figure S4 | Cycling *ex-situ* Mn 2p ½ XPS Studies of $LaMnO_{3\pm\delta}$: Carbon-free electrodes of r-$LaMnO_{2.91}$ (**a)** and $LaMnO_{3.09}$ (**b)** were cycled between 25-500 times and then characterized using XPS. **c,** Both electrodes were found to have an initial increase of surface manganese (compared to the relative atomic percent of lanthanum based on the La 4p 3/2 contribution) concomitant with an increase in the oxidation state to Mn^{4+} due to the addition of electrolyte oxygen ions. Because of this, it is likely that oxygen diffusion rates are greatly enhanced at the surface along grain boundaries leading to regions where oxygen intercalation is rapid and pseudocapacitive rather than purely faradaic.

DOI: 10.1038/NMAT4000

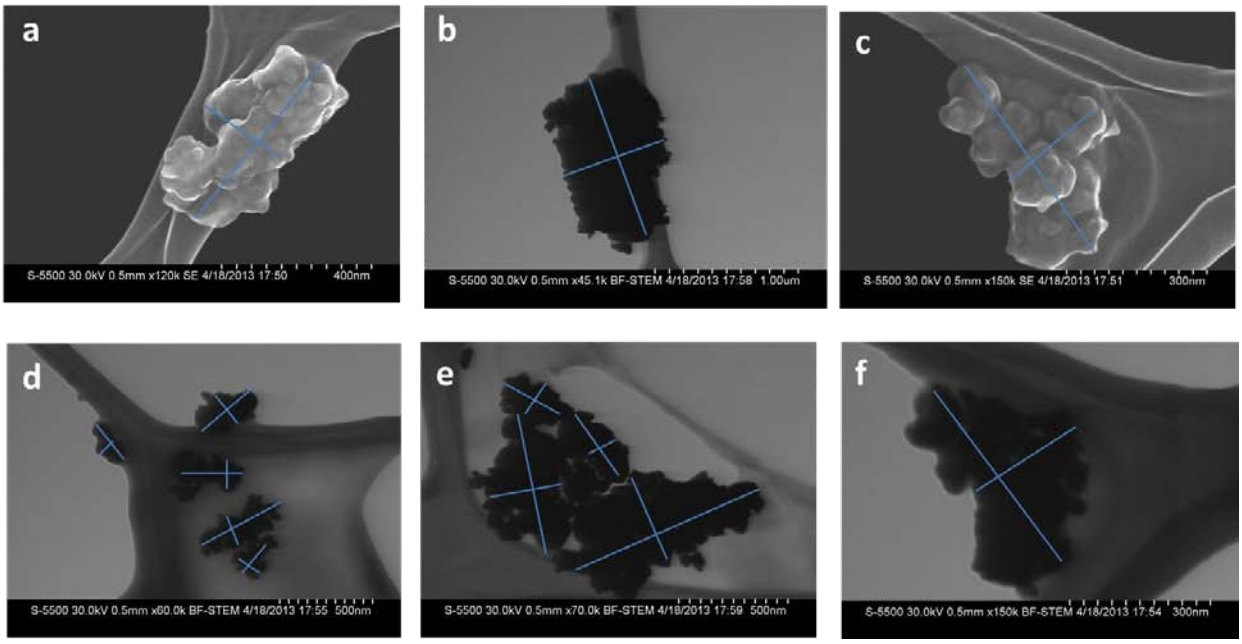

Figure S5 | Particle thickness analysis for diffusion rate calculation: The thickness of the particles was approximated by taking the average of lateral dimension measurements of $LaMnO_{3.09}$ from SEM images. The average thickness corresponded to 380±90 nm with an N value of 26.

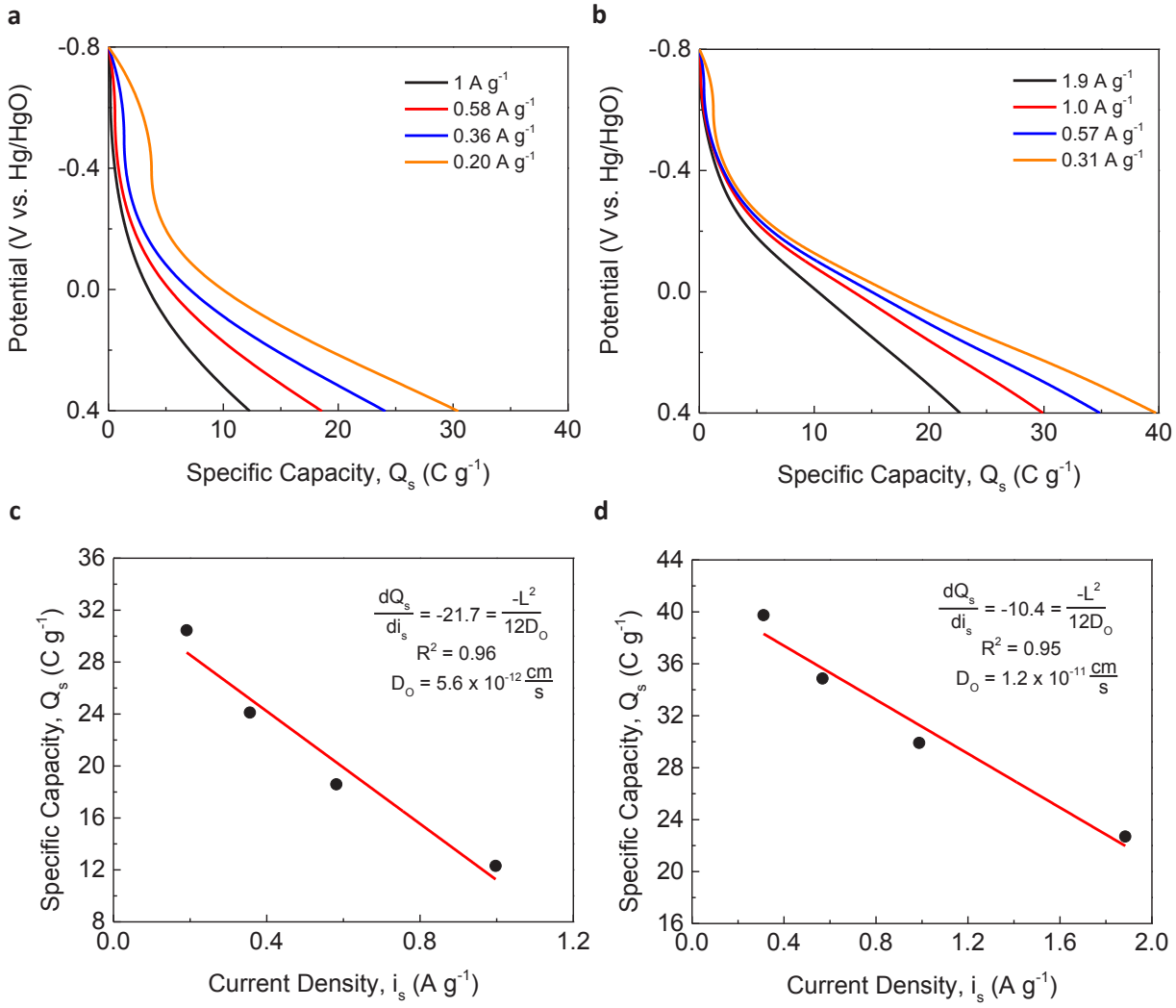

Figure S6 | Diffusion rate calculations on unsupported $LaMnO_{3\pm\delta}$: Calculation of the diffusion rates for **a,c.** $LaMnO_{3.09}$ and **b,d**. r-$LaMnO_{2.91}$. The potential versus capacity plots presented in **a,b** are calculated from integration of the oxidation current from the CV's presented in S4a and S4b. The sharp drop in potential at low capacity changes is indicative of the ohmic drop in both samples because carbon was not included as a conductive support in these samples. The thickness, *L*, was approximated from Figure S5.

DOI: 10.1038/NMAT4000

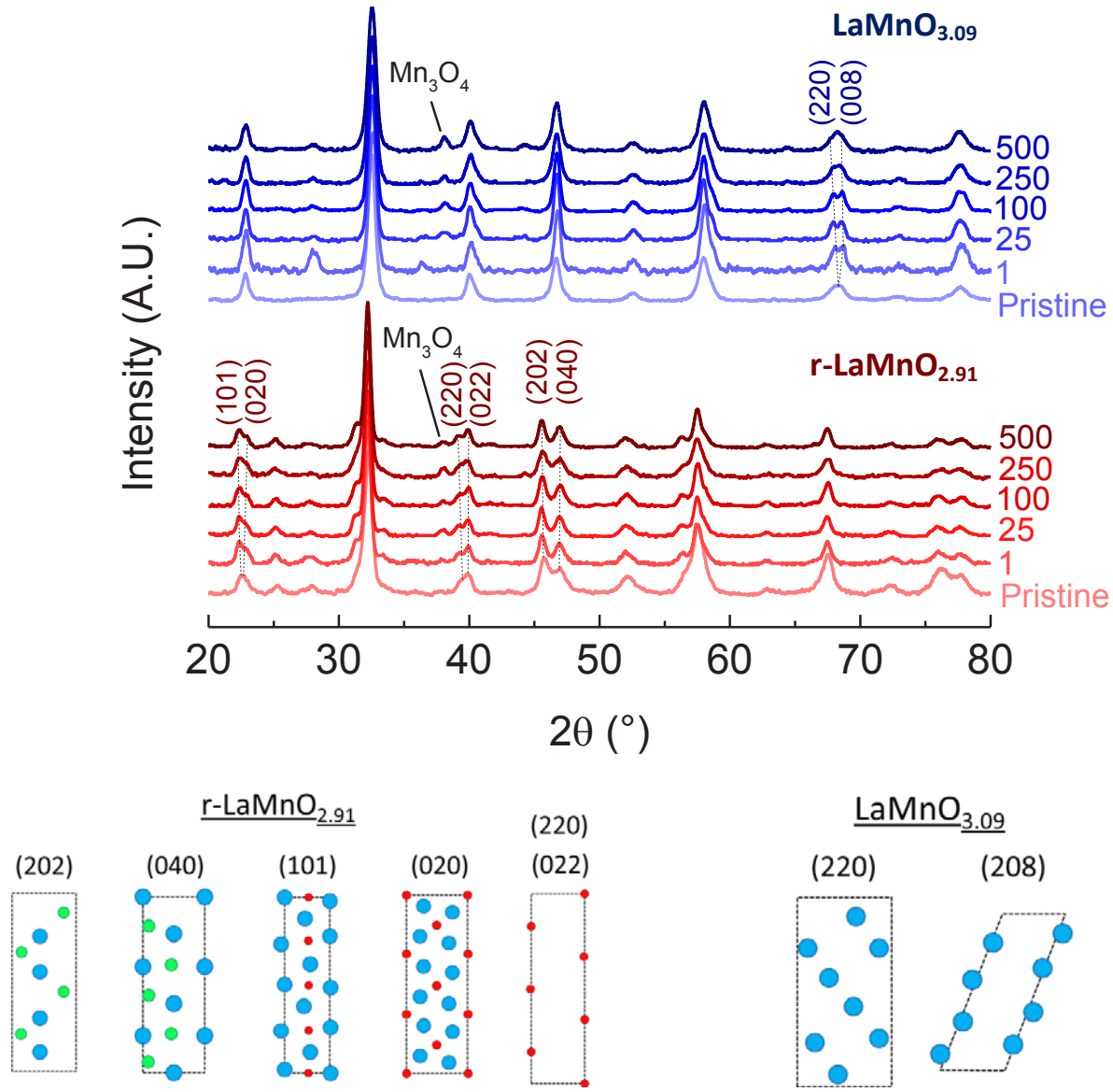

Figure S7 | Cycling *ex-situ* XRD Studies of $LaMnO_{3\pm\delta}$: The degree to which oxygen intercalation extended into the bulk was investigated through XRD on cycled electrode materials. However, over the course of cycling it was found that there were minimal changes in the bulk structure. The diffraction peaks that underwent the most drastic changes have been labeled in the figure and interestingly correspond to lattice planes that contain either only oxygen atoms, or direct

pathways for oxygen diffusion.[6-11] In addition, a peak at 38° corresponding to Mn_3O_4 grew in over cycling in both samples, which is likely formed during the removal of surface oxygen which results in Mn^{2+} necessary to form the spinel phase. The lack of significant changes in the XRD spectrum is expected from previous work on $LaMnO_{3\pm\delta}$ materials, where vacancies are randomly distributed throughout the crystal structure but do not lead to significant distortions in atomic arrangements and lattice spacings.[6-10] In combination with the XPS results, it is concluded that oxygen intercalation is dominated by the surface of the electrodes, but due to the high oxygen diffusion rates and high specific capacities found in this work, that the oxygen intercalation extends more deeply into the crystal than just the pure surface.

DOI: 10.1038/NMAT4000

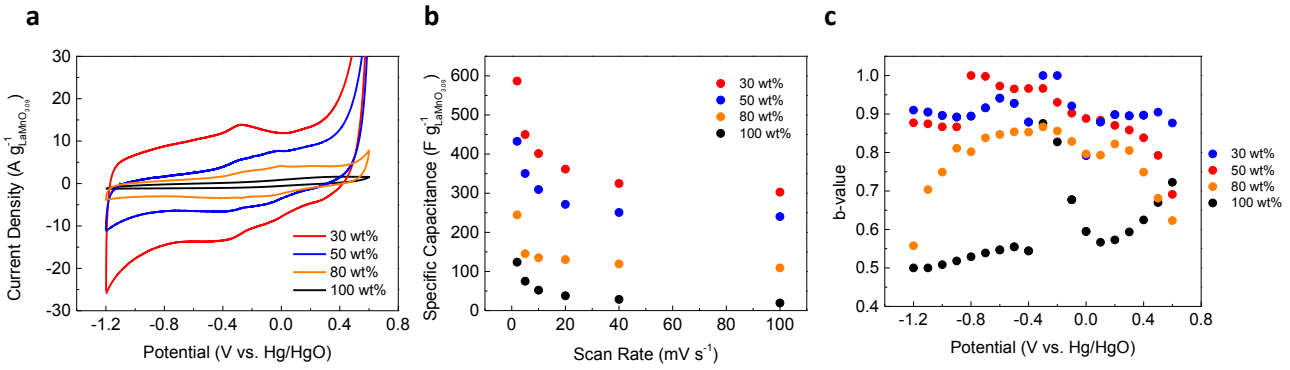

Figure S8 | Effect of weight loading on the capacitive contributions of $LaMnO_{3.09}$. a, Cyclic voltammograms at 100 mV s^{-1} for various weight loadings of $LaMnO_{3.09}$ on N-OMC. The contribution of the carbon support to the current and the capacitance have been subtracted. The sharp increase in current at ~0.2V vs. Hg/HgO corresponds to the oxygen evolution reaction on $LaMnO_{3.09}$ in alkaline electrolytes. **b,** Specific capacitance versus scan rate for $LaMnO_{3.09}$ at various weight loadings. **c**, b-value analysis of $LaMnO_{3.09}$ at different mass loadings. The b-value peaks at approximately E = -0.3 V vs. Hg/HgO for all mass loadings which corresponds to the position of the redox peaks in the cyclic voltammograms. *In all of these figures, the current and capacitance contributions of the carbon support have been subtracted out to clearly demonstrate the electrochemical characteristics of $LaMnO_{3.09}$.

The effect of weight loading on carbon and the capacitive contribution to the current was investigated using a power-law dependence or b-value analysis method according to equation (S1):[12]

$$i = av^b \quad \text{(S1)}$$

where *i* (A) is the current produced by $LaMnO_{3.09}$, *a* is a constant, *v* is the scan rate (V s^{-1}), and *b* is indicative of the capacitive contribution to the current obtained from a power fit of the current versus scan rate. Pure diffusion controlled reactions correspond to a b-value of 0.5 while a b-value of 1 is indicative of a purely capacitive current, including intercalation based pseudocapacitance. An extended potential window of -1.2 to 0.6 V vs. Hg/HgO was used in order to encompass the redox peaks at all mass loadings, where resistive effects result in a substantial increase in the overpotential for oxygen intercalation in high weight loadings of $LaMnO_{3\pm\delta}$. As seen in Figure 4, the low electronic conductivity of $LaMnO_3$ requires the use of a substantial amount of carbon, ~70%, to achieve significant pseudocapacitive behavior. However, the b-value analysis peaks at the approximate potential of -0.3V vs. Hg/HgO for all samples, corresponding to the $E_{1/2}$ of the redox peaks present in the 30 wt% loading samples.

DOI: 10.1038/NMAT4000

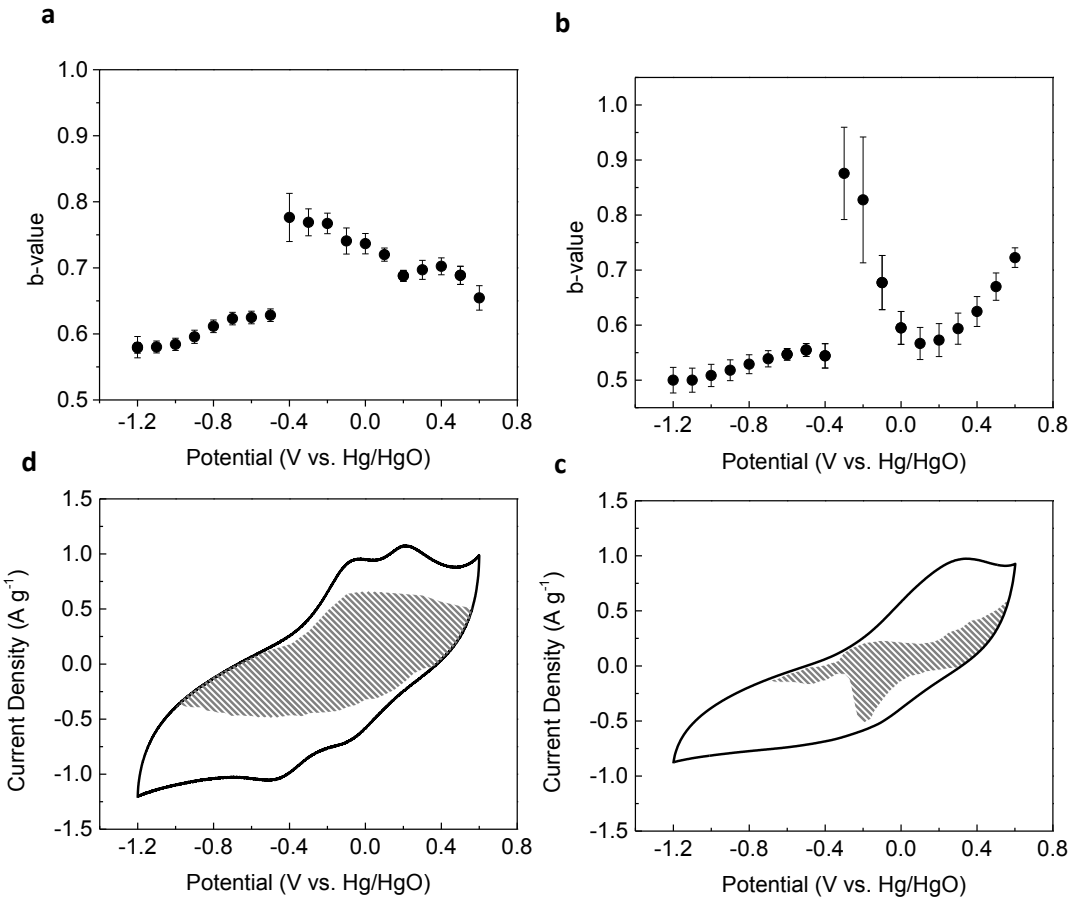

Figure S9 | b-value analysis of $LaMnO_{3\pm\delta}$: a,b. b-values for r-$LaMnO_{2.91}$ (**a**) and $LaMnO_{3.09}$ (**b**). **c,d**. CV's of r-$LaMnO_{2.91}$ (**c**) and $LaMnO_{3.09}$ (**d**). The shaded grey areas show the capacitive current envelope. The presence of a peak in the capacitance values at E ~ -0.3V vs. Hg/HgO corresponds well with the $E_{1/2}$ of the reaction for oxygen intercalation.

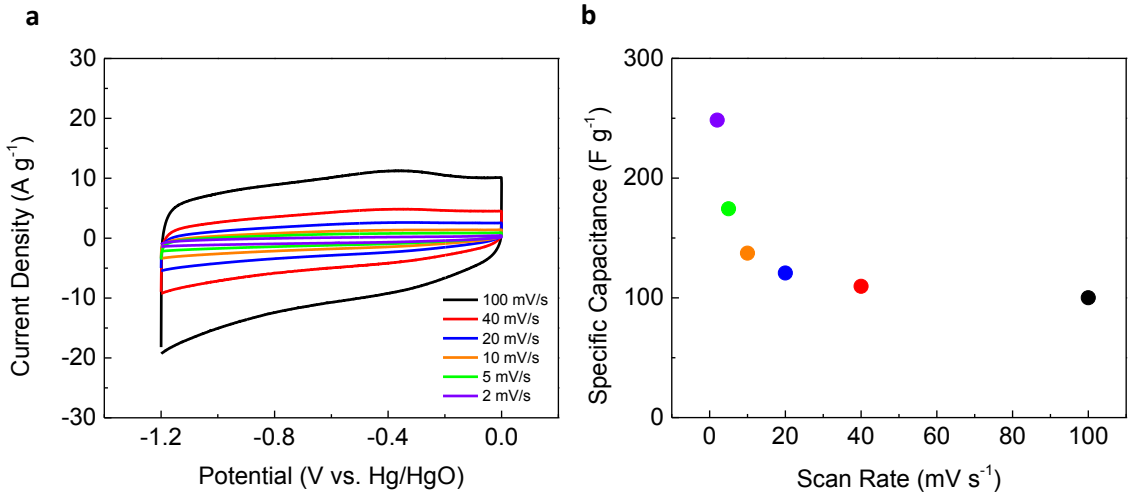

Figure S10 | Capacitive contributions of N-OMC Support: a, Cyclic voltammogram of nitrogen-doped ordered mesoporous carbon support (N-OMC) at various scan rates. **b,** Specific capacitance versus scan rate for N-OMC. Importantly there is an absence of redox peaks at $E_{1/2}$ ~ -0.3V vs. Hg/HgO which are present in the $LaMnO_{3\pm\delta}$ samples.

DOI: 10.1038/NMAT4000

Supplementary References:

1. Mickevicius, S. *et al.* Investigation of Epitaxial $LaNiO_{3-X}$ Thin Films by High-Energy XPS. *J. Alloys Compd.* **423**, 107-111 (2006).
2. De Asha, A., Critchley, J. & Nix, R. Molecular Adsorption Characteristics of Lanthanum Oxide Surfaces: The Interaction of Water with Oxide Overlayers Grown on Cu (111). *Surf. Sci.* **405**, 201-214 (1998).
3. Djurfors, B., Broughton, J., Brett, M. & Ivey, D. Electrochemical Oxidation of Mn/Mno Films: Formation of an Electrochemical Capacitor. *Acta Mater*. **53**, 957-965 (2005).
4. Sunding, M. *et al.* XPS Characterisation of *in situ* Treated Lanthanum Oxide and Hydroxide Using Tailored Charge Referencing and Peak Fitting Procedures. *J. Electron Spectrosc.* **184**, 399-409 (2011).
5. Chen, J. *et al.* The Influence of Nonstoichiometry on $LaMnO_3$ Perovskite for Catalytic NO Oxidation. *Applied Catalysis B: Environmental* **134**, 251-257 (2013).
6. Mori, T., Inoue, K. & Kamegashira, N. Phase behavior in the system $La_xSr_{1-x}MnO_{(5+x)/2}$ (x=0.8-1.0) with trivalent state of manganese ion. *J. Alloy Compd.* **308**, 87-93 (2003).
7. Ng-Lee, Y. *et al.* Low-temperature synthesis, structure and magnetoresistance of submicrometric $La_{1-x}K_xMnO_{3+\delta}$ perovskites. *J. Mater. Chem.* **7**, 1905-1909 (1997).
8. Barnabé, A. *et al.* Low temperature synthesis and structural characterization of over-stoichiometric $LaMnO_{3+\delta}$ perovskites. *Mat. Res. Bull.* **39**, 725-735 (2004).

9. Norby, P., Krogh Anderson, I. G. & Krogh Anderson, E. The Crystal Structure of Lanthanum Manganate(III), $LaMnO_3$, at Room Temperature and at 1273K under N_2. *J. Solid State Chem.* **119**, 191-196 (1995).

10. Sakai, N., Fjellvåg, H. & Lebech, B. Effect of Non-Stoichiometry on Properties of $La_{1-t}MnO_{3+\delta}$. Part II. Crystal Structure. *Acta Chem. Scand.* **51**, 904-909 (1997).

11. Momma, K. & Izumi, F. *Vesta 3* for three-dimensional visualization of crystal, volumetric and morphology data. *J. Appl. Cryst.* **44**, 1272-1276 (2011).

12. Brezesinski, T., Wang, J., Tolbert, S. H. & Dunn, B. Ordered mesoporous α-MoO_3 with iso-oriented nanocrystalline walls for thin-film pseudocapacitors. *Nature Mater.* **9**, 146-151 (2010).